Title
AN UPDATE ON DROPLET MODEL CHARGE DISTRIBUTIONS

Authors
Myers, W.D.
Schmidt, K-H.

Publication Date
1983-04-01

LBL-15446
Preprint

Lawrence Berkeley Laboratory
UNIVERSITY OF CALIFORNIA

Submitted to Nuclear Physics

AN UPDATE ON DROPLET MODEL CHARGE DISTRIBUTIONS

William D. Myers and Karl-Heinz Schmidt

April 1983

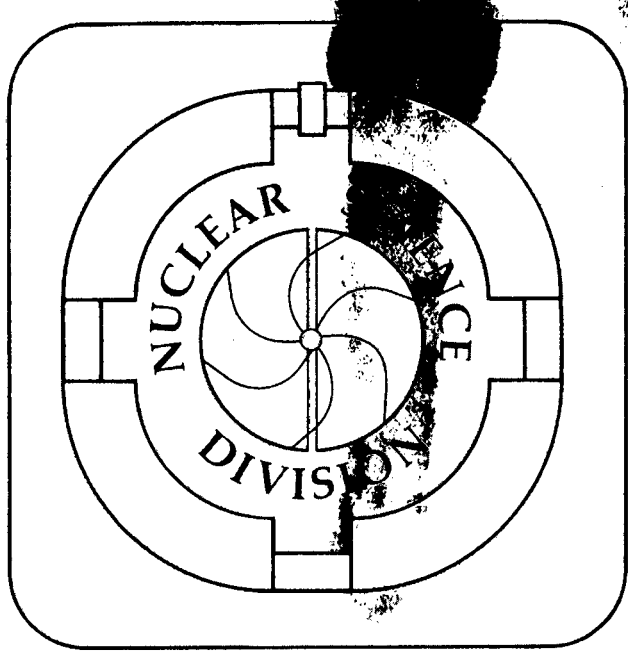

Prepared for the U.S. Department of Energy under Contract DE-AC03-76SF00098

DISCLAIMER

LBL-15446

An Update on Droplet Model Charge Distributions

William D. Myers

Nuclear Science Division, Lawrence Berkeley Laboratory
University of California, Berkeley, CA 94720

and

Karl-Heinz Schmidt

Gesellschaft für Schwerionenforschung
D-6300 Darmstadt 11, West Germany

Abstract

The Droplet Model expressions for calculating various moments of the nuclear charge distribution are given. There are contributions to the moments from the size and shape of the system, from the internal redistribution induced by the Coulomb repulsion, and from the diffuseness of the surface. A case is made for the use of diffuse charge distributions generated by convolution as an alternative to Fermi-functions.

This work was supported by the Director, Office of Energy Research, Division of Nuclear Physics of the Office of High Energy and Nuclear Physics of the U.S. Department of Energy under Contract DE-AC03-76SF00098.

Introduction

The Droplet Model provides a comprehensive description of a number of macroscopic aspects of nuclei such as the binding energy and the associated potential energy as a function of the collective coordinates[1-3]). It also provides a basis for a rather detailed description of both the neutron and proton spatial distributions. In ref. [4]) Myers and Swiatecki discuss the problem of the "neutron skin" and give references to the earlier work on Droplet Model density distributions. More recently, the present authors[5-7] and others[8,9]) have concentrated on comparing the Droplet Model predictions of RMS charge radii with the large number of excellent measurements of radii and isotope shifts that are currently becoming available. It is our purpose here to bring together some of these results and to extend the discussion so as to provide an update on the status of the Droplet Model predictions.

Droplet Model Density Distributions

The Droplet Model predictions for nuclear density distributions differ from those of the Liquid Drop Model in two important ways. The most important difference is that the equivalent sharp radii of the neutron and proton distributions are determined by minimizing the macroscopic energy of the system. This procedure results in a prediction that light nuclei are squeezed slightly by the surface tension and that most nuclei have a neutron skin because the neutron distribution is slightly larger than the proton distribution for neutron excess nuclei. The other difference is the predicion of a small amount of bulk redistribution under the influence of the repulsive Coulomb force.

Since the Droplet Model expressions governing these phenomena have been given so often[1-4]), the next section will be as brief as possible commensurate with completeness.

The Size

The first step in constructing the Droplet Model nuclear density distributions is to calculate the size of the system (neutrons and protons together) from the expression

$$R = r_o A^{1/3} (1 + \bar{\epsilon}) \quad , \tag{1}$$

where

$$\bar{\epsilon} = \left(-2a_2 A^{-1/3} B_s + L\,\bar{\delta}^2 + c_1 Z^2 A^{-4/3} B_c\right)/K \quad , \tag{2}$$

$$\bar{\delta} = \frac{I + \frac{3}{16}(c_1/Q) Z A^{-2/3} B_v}{1 + \frac{9}{4}(J/Q) A^{-1/3} B_s} \quad , \tag{3}$$

and

$$I = (N-Z)/A \quad , \tag{4}$$

(The quantity B_s is the ratio of the surface area of a deformed nucleus to that of a sphere with equal volume, B_c is the analogous term for the Coulomb energy, and B_v is associated with variations in the Coulomb potential over the surface when a nucleus is deformed.)

One currently accepted set of values for the Droplet Model coefficients that appear here is[3])

r_o = 1.18 fm, the nuclear radius constant,

b = 0.99 fm, the nuclear diffuseness,

$c_1 = \frac{3}{5}(e^2/r_o)$ = 0.7322 MeV, the Coulomb energy coefficient,

a_2 = 20.69 MeV, the surface energy coefficient,

J = 36.8 MeV, the symmetry energy coefficient,

Q = 17 MeV, the effective surface stiffness,

K = 240 MeV, the compressibility coefficient, and

L = 100 MeV, the density symmetry coefficient.

Once the mean radius R has been calculated the neutron skin thickness can be obtained from the expression

$$t = \frac{2}{3} R\ (I - \bar{\delta})/B_s \quad , \tag{6}$$

The separate effective sharp radii for the neutron and proton distributions can be calculated from the expressions,

$$\begin{aligned} R_n &= R + \frac{Z}{A} t \quad , \\ R_z &= R - \frac{N}{A} t \quad . \end{aligned} \tag{7}$$

The Shape

A simple, useful representation for the shape of the density distribution is in terms of Legendre polynomials,

$$r = nR\ (1 + \alpha_2 P_2 + \alpha_4 P_4 + \alpha_6 P_6 + \ldots) \tag{8}$$

where volume normalization is insured by setting

$$n = (1 - \frac{1}{5}\alpha_2^2 - \frac{2}{105}\alpha_2^3 + \frac{2}{25}\alpha_2^4 - \frac{2}{35}\alpha_2^2\alpha_4 - \frac{1}{9}\alpha_4^2 \ldots). \tag{9}$$

In terms of this expansion the shape dependences above are

$$\begin{aligned} B_s &= 1 + \frac{2}{5}\alpha_2^2 - \frac{4}{105}\alpha_2^3 - \frac{66}{175}\alpha_2^4 - \frac{4}{35}\alpha_2^2\alpha_4 + \alpha_4^2 \ldots \\ B_c &= 1 - \frac{1}{5}\alpha_2^2 - \frac{4}{105}\alpha_2^3 + \frac{51}{245}\alpha_2^4 - \frac{6}{35}\alpha_2^2\alpha_4 - \frac{5}{27}\alpha_4^2 \ldots \\ B_v &= 1 - \frac{1}{5}\alpha_2^2 - \frac{2}{105}\alpha_2^3 - \frac{253}{1225}\alpha_2^4 - \frac{4}{105}\alpha_2^2\alpha_4 + \frac{4}{9}\alpha_4^2 \ldots \quad . \end{aligned} \tag{10}$$

In these expressions and those that follow, we have chosen to retain only terms up to order ϵ^4, where the coeffficients α_2, α_4, and α_6 are regarded as being of relative order ϵ, ϵ^2, and ϵ^3.

The Redistribution

Once the Droplet Model size of the distribution has been determined, and some other source has been consulted for information about the shape (for example, a table of measured values or the recent Möller and Nix compilation of predicted deformations[10,11]), we can proceed to the next level of refinement. The protons (and neutrons to some extent) are pushed toward the surface by the Coulomb repulsion, and the small increase in binding that results is included in the Droplet Model energy expression. The corresponding change in the density is given by[2]

$$\tilde{\rho}_2 = -\frac{1}{2}\rho_o\left(\frac{9}{2K} \mp \frac{1}{4J}\right)e\tilde{v} \quad , \tag{11}$$

where $\tilde{v}$ is the deviation of the Coulomb potential from its average value over the bulk.

For a spherical distribution[2]),

$$\begin{aligned} v &= \frac{Ze}{R_z}\left[\frac{3}{2} - \frac{1}{2}\left(\frac{r}{R}\right)^2\right] \quad , \\ \bar{v} &= \frac{6}{5}\frac{Ze}{R_z} \quad , \\ \tilde{v} &= \frac{1}{2}\frac{Ze}{R_z}\left[\frac{3}{5} - \left(\frac{r}{R}\right)^2\right] \quad , \end{aligned} \tag{12}$$

and for a distribution whose shape is given by Eq. (8) above[12],

$$v = \frac{Ze}{R_z}\left(-\frac{1}{2}\zeta^2 + \frac{3}{2}\sum_{i=0,2,4,6} C_i \zeta^i P_i\right) \quad , \tag{13}$$

$$\bar{v} = \frac{Ze}{R_z}\left(\frac{6}{5} B_c\right) \quad , \tag{14}$$

$$\tilde{v} = \frac{Ze}{R}\left(-\frac{1}{2}\zeta^2 + \frac{3}{2}\sum_{i=0,2,4,6} D_i \zeta^i P_i\right) \quad , \tag{15}$$

where $\zeta = r/nR_z$ and the C's and D's are given in the appendix.

The change in the proton distribution due to redistribution can be written

$$\tilde{\rho}_z = \frac{1}{2}\rho_o C' f(r) \quad , \tag{16}$$

where

$$C' = \frac{1}{2}\left(\frac{9}{2K} + \frac{1}{4J}\right)\frac{Ze^2}{R_z} \quad , \approx 0.0156\ ZA^{-1/3} \ . \tag{17}$$

For a spherical nucleus

$$f(r) = [(r/R_z)^2 - 3/5] \quad , \tag{18}$$

and for a deformed nucleus

$$f(\zeta) = \left(\zeta^2 - 3\sum_{i=0,2,4,6} D_i \zeta^i P_i\right) \ . \tag{19}$$

The redistribution creates a central depression in the proton distribution that increases all the radial moments. It also increases the charge on the ends of a deformed shape, resulting in an increase in the quadrupole, hexadecapole, and other even order multipole moments.

The Diffuseness

Once the size, the shape, and the redistribution have been combined, the last step in the determination of the Droplet Model prediction for the density distribution is to add the diffuseness. The customary procedure of using Fermi functions is awkward and inconvenient (especially when the density is deformed and redistributed) and so we will use convolution to create the diffuseness. When a normalized, spherically symmetric, short-ranged function is folded into our sharp-surfaced distribution the resulting diffuse distribution still has the same volume integral (contains the same number of particles). What is most significant is the fact that the multipole moments of the distribution are unchanged and the radial moments (and moment of inertia) simply increase by a known constant[13,14]). So, we do not have to actually perform the convolution integral, unless we want to plot the density distribution itself.

A proposal for creating the diffuseness in this way was made by Helm[15]), in connection with the interpretation of elastic electron scattering measurements. More recent work along these same lines has been done by Friedrich and Voegler[8,9]) They find that "Helm Model" effective sharp radii extracted from experiment behave much as the Droplet Model says they should and that the variance of the gaussian folding function,

$$g(r) = (2\pi\sigma^2)^{-3/2} \exp(-r^2/2\sigma^2) \tag{20}$$

is nearly constant throughout the periodic table except for some small evidence of shell structure.

It should be mentioned in passing that $\sigma = b$ and that the geometrical relationships between the surface location C, the effective sharp radius R, the effective RMS radius Q, and the surface width b have been discussed by

Süssmann[16]) and other authors[14,17]). The advantages of the folding method have also received recent attention from Krappe[18]).

Radial Moments

The most frequently measured quantity, the mean square radius $\langle r^2 \rangle$, can be calculated from the expression

$$\langle r^2 \rangle = \langle r^2 \rangle_u + \langle r^2 \rangle_r + \langle r^2 \rangle_d \quad , \tag{21}$$

where (the subscript Z, indicating protons, is dropped here since these expressions are completely general)

$$\langle r^2 \rangle_u = \frac{3}{5} R^2 \left(1 + \alpha_2^2 + \frac{10}{21} \alpha_2^3 - \frac{27}{35} \alpha_2^4 + \frac{10}{7} \alpha_2^2 \alpha_4 + \frac{5}{9} \alpha_4^2 + \ldots\right) \tag{22}$$

is the contribution from the size of the uniform distribution and its shape. The next term,

$$\langle r^2 \rangle_r = \frac{12}{175} C'R^2 \left(1 + \frac{14}{5} \alpha_2^2 + \frac{28}{15} \alpha_2^3 - \frac{29}{5} \alpha_2^4 + \frac{116}{15} \alpha_2^2 \alpha_4 + \frac{70}{26} \alpha_4^2 + \ldots\right) \tag{23}$$

is the contribution from the redistribution, and its shape dependence. The last term,

$$\langle r^2 \rangle_d = 3\sigma^2 \quad \text{or} \quad 3b^2 \tag{24}$$

is the contribution from the diffuseness. It is interesting to note that the diffuseness correction has no shape dependence and that it is the same for all nuclei (so long as we assume that the diffuseness itself is a constant).

In order to assess the relative importance of the different terms we can consider the example of ^{238}U. The spherical Droplet Model value of R_z is 7.030 fm, and this becomes 7.027 fm when the effect of deformation [using the

values $\alpha_2 = 0.1395$, $\alpha_4 = 0.0652$, and $\alpha_6 = 0.0024$ provided by Möller[8])] on the size of the distribution is included via the B's Eq. (10). The mean square radius of a uniform distribution with this shape and a sharp surface is 29.6273 (1+0.02462) fm^2, where the first part comes from the size and the second from the shape. The redistribution contribution is 0.8790 fm^2, and the diffuseness correction is 2.9403 fm^2, for a total of 34.1760 fm^2. The predicted RMS radius is 5.8406 fm, which is to be compared with the experimental value of 5.843 ± 0.012 fm [19]).

In fig. 1 a broad comparison is made between the measured values and the values calculated using the Droplet Model expression (21) and the calculated deformations of Möller and Nix[11]). In this comparison the compilation of experimental RMS radii of Angeli and Csatlos[19]) was extended by RMS radii and isotope shifts of isotopes of potassium[20,21]), calcuium[21,22]), scandium[21]), titanium[21]), vanadium[21]), chromium[21]), manganese[21]), iron[21]), krypton[23]), rubidium[24]), palladium[25]), cadmium[26,27]), xenon[23]), cesium[28]), barium[29,30]), dysprosium[31]), erbium[31]), ytterbium[31]), mercury[32]), and lead [33]). Isotopes of the same element are connected by a line. The error bar at the top of the figure represents the typical uncertainty of the absolute RMS radii, which are determined only for some stable isotopes, and the RMS radii of isotopic chains are then linked by rather accurate isotope shifts. As a consequence the groups of points that lie away from the main concentration of values correspond to single measurements, rather than a number of supporting deviations as one might have thought at first. The strong odd-even staggering around A = 103 refers to mercury isotopes. It can be explained by shortcomings of the theoretical prediction of the nuclear deformation. The experimentally observed sudden transition to strong deformation is not reproduced by the calculation. The light vertical lines are located at the neutron magic numbers 28, 50, 82, and 126.

They serve to bring our attention to shell-related deviations at 28 and 50 These deviations may be associated with radial shell effects or they may simply reflect differences between the actual shapes of nuclei in these regions and the theoretical shapes that were used in the calculations. The deviations are summed in the histogram at the right of the figure, and inspection shows that the centroid is at about -0.015 fm suggesting that the Droplet Model radius constant r_o should probably be decreased by (3/10) of a percent.

In fig. 2 another comparison between the measured and calculated values is given, this time without corrections for deformation. The structure imposed on the RMS radii by the increase and then decrease in deformation that occurs as one moves from one magic number to the next can be clearly seen. This sort of structure is almost completely absent from the previous figure suggesting that all the shell effects are shape effects and that there is little evidence for volume (or diffuseness) shell effects.

Figure 3 displays the differences that remain when the appropriate deformation corrections are made but a Liquid Drop Model expression is used for the size of the proton distribution instead of the Droplet Model expression. In this figure

$$RMS_{calc} = \sqrt{\frac{3}{5}} \left(1.15 + 1.80\ A^{-2/3} - 1.20\ A^{-4/3}\right) A^{1/3}\ \text{fm} \quad , \qquad (25)$$

corresponding to an equivalent sharp radius of $1.15\ A^{1/3}$ fm and a diffuseness b of 0.98 fm. The steep downward slope of isotopic sequences that is seen here (but not in fig. 1) is due to the LDM neglect of the effects of the neutron skin on charge radii. Another way of displaying this effect can be seen in fig. 4. Here, the measured RMS radii have been converted to equivalent sharp radii by the approximate procedure of multiplying by (R_D/RMS_D), where R_D is the

Droplet Model predicted equivalent sharp radius, and RMS_D is the Droplet Model prediction for the RMS radius with all the diffuseness deformation and redistribution effects included. A straight line has then been fitted to isotopic sequences and the slope of this line ΔR_n (multiplied by $A^{2/3}$) has been plotted against the Z value for the sequence. The Liquid Drop model would predict that this quantity should always have the constant value 1/3 r_o (as is indicated by the dotted line in the figure). The data are seen to cluster about the dashed line representing the Droplet Model predction. The solid horizontal line at $\Delta R_n * A^{2/3} = 0$ corrresponds to the idea that charge radii depend only on the value of Z, as has sometimes been advocated. The data used here include some isotopic sequences that could not be used in the previous figures because they consist of only isotope shifts without any absolute measurement. In addition, some of the sequences from the previous figures have been omitted here because they consist of fewer than four points.

Further comparison can be made with the more recent extensive measurements of cesium isotopes reported in ref. [28]). Figure 5 shows how well these measured relative mean square radii are reproduced by the calculations. The agreement below the magic number 82 is quite striking, corresponding as it does to differences of a few attometers (1 am = 1 millifemtometer = 10^{-18} meter). The poorer agreement beyond the magic number may be associated with deficiencies in the calculated deformations that were used.

Another similar comparison is made in fig. 6, for the rubidium isotopes from ref. [24]). In this case the agreement is best at some distance from the magic number 50, but the calculated values decrease abruptly to approximately the undeformed Droplet Model value on both sides of the magic number N = 50. (A similar, but less striking effect can be seen in the previous figure.) The reason for these differences is quite interesting, and it is discussed at some

length in ref. [34]) as well as in ref. [35]) where an attempt was made to understand the measured values in terms of Hartree-Fock calculations. Briefly, the difference appears to have its origin in the fact that the RMS radii depend on $\langle\alpha_i^2\rangle$. In the transition region between the magic number and the solidly established deformations there exists a region in which zero point motion in the collective coordinates generates a large value for $\langle\alpha^2\rangle$ even though $\langle\alpha\rangle \approx 0$. One consequence of this effect is that better agreement between measured and calculated RMS radii can be obtained if measured values of $\langle\alpha_i^2\rangle$ are used rather than assuming that $\langle\alpha_i^2\rangle \approx \langle\alpha_i\rangle_{calc}^2$ as we have above.

Multipole Moments

Using the definition,

$$Q_\ell = 2 \int r^\ell P_\ell \, d^3r \quad , \tag{26}$$

we can derive expressions for the multipole moments analogous to eq. (21). Thus,

$$Q_\ell = Q_\ell^u + Q_\ell^r + Q_\ell^d \quad , \tag{27}$$

where Q_ℓ^u is the contribution from the uniform distribution, Q_ℓ^r the contribution from redistribution, and (as we mentioned before) Q_ℓ^d is the contribution from the diffuseness, which is identically zero. For the quadrupole moment,

$$Q_2^u = \frac{6}{5} ZR^2 \left(\alpha_2 + \frac{4}{7}\alpha_2^2 - \frac{1}{7}\alpha_2^3 - \frac{94}{231}\alpha_2^4 + \frac{8}{7}\alpha_2\alpha_4 + \frac{72}{77}\alpha_2^2\alpha_4 + \frac{200}{693}\alpha_4^2 + \ldots\right), \tag{28}$$

$$Q_2^r = \frac{48}{175} C' ZR^2 \left(\alpha_2 + \frac{6}{7}\alpha_2^2 - \frac{4}{5}\alpha_2^3 - \frac{1984}{1155}\alpha_2^4 + \frac{50}{21}\alpha_2\alpha_4 + \frac{28}{11}\alpha_2^2\alpha_4 + \frac{1600}{2079}\alpha_4^2 + \ldots\right) \quad , \tag{29}$$

and for the hexadecapole moment,

$$Q_4^u = \frac{2}{3} ZR^4 \left(\frac{54}{35}\alpha_2^2 + \frac{108}{77}\alpha_2^3 + \frac{8154}{25025}\alpha_2^4 + \alpha_4 + \frac{120}{77}\alpha_2\alpha_4 + \frac{19828}{5005}\alpha_2^2\alpha_4 + \frac{486}{1001}\alpha_4^2 + \frac{270}{143}\alpha_2\alpha_6 + \ldots\right) , \tag{30}$$

$$Q_4^r = \frac{112}{495} C'ZR^4 \left(\frac{81}{49}\alpha_2^2 + \frac{34344}{18865}\alpha_2^3 - \frac{21435516}{15940925}\alpha_2^4 + \alpha_4 + \frac{160}{77}\alpha_2\alpha_4 + \frac{19508026}{3188185}\alpha_2^2\alpha_4 + \frac{5427}{7007}\alpha_4^2 + \frac{35235}{13013}\alpha_2\alpha_6 + \ldots\right) . \tag{31}$$

For ^{238}U (using the α's mentioned earlier) the predicted moments are

$$Q_2 = 8.8768 + 0.5444 = 9.4212 \text{ barn} , \tag{32}$$

and

$$Q_4 = 1.8053 + 0.1620 = 1.9673 \text{ barn}^2 , \tag{33}$$

which are to be compared with the corresponding measured values of 9.04 ± 0.06 barn and 2.21 ± 0.46 barn^2 [from ref. [36])]. The calculated value of the quadrupole moment is increased 6% and the hexadecapole moment 9% by the redistribution of charge.

Summary

We have extended the usual Droplet Model predictions of charge moments to incude deformation and redistribution contributions. When compared with the measured values the accuracy obtainable by this method seems to be about 0.01 fm (or 10 am), which corresponds to 0.2% in the RMS radius for a heavy nucleus. This is almost as good as the 0.1% accuracy (1 MeV out of 1000 MeV) that can be obtained for the binding energy, when the macroscopic approach is supplemented by shell corrections.

We also showed that the Liquid Drop Model fails to correctly predict the changes in charge radii along isotopic sequences. The excellent agreement that is found when the Droplet Model is used is associated with the neutron skin that develops for neutron-rich nuclei. The model coefficients governing this effect and the radius constant itself were all determined from fitting only to nuclear masses and fission barriers. Consequently, some improvement could be expected in the predictions if the measured values of the radii were to be included in the fitting procedure.

Finally, we showed how the Droplet Model redistribution affects the relation between the shape of a nucleus and its charge multipole moments. The size of this new term is comparable to the accuracy with which these moments are known.

The authors wish to acknowledge contributions made by Rainer Hasse, Peter Möller, Wladek Swiatecki, and G. Ulm. They also wish to express their appreciation to the authors who made available the most recent measured values for a number of nuclear RMS radii. This work was supported by the Director, Office of Energy Research, Division of Nuclear Physics of the Office of High Energy and Nuclear Physics of the U.S. Dept. of Energy under Contract DE-AC03-76SF-00098.

References

1. W.D. Myers and W.J. Swiatecki, Ann. Phys. (NY) 55 (1969) 395-505
2. W.D. Myers and W.J. Swiatecki, Ann. Phys. (NY) 84 (1974) 186-210
3. W.D. Myers, Droplet Model of Atomic Nuclei (IFI/Plenum Data Co., New York, 1977)
4. W.D. Myers and W.J. Swiatecki, Nucl. Phys. A336 (1980) 267-78
5. W.D. Myers, Proc. XIX Int. Winter Meeting on Nuclear Physics, Bormio, Italy, January 1981, p. 336-40

6. W.D. Myers and K.-H. Schmidt, CERN 81-09, Proc. 4th Int. Conf. on Nuclei far from Stability, Helsingor, Denmark, June 1981, p. 90-2
7. W.D. Myers, Proc. Conf. on Lasers in Nuclear Physics, Oak Ridge, Tenn., April 1982
8. J. Friedrich and N. Voegler, Phys. Rev. Lett. 47 (1981) 1385-8
9. J. Friedrich and N. Voegler, Nucl. Phys. A373 (1981) 192-224
10. P. Möller and J.R. Nix, At. Data Nucl. Data Tables 26 (1981) 165-96
11. P. Möller, private communication, March 1982.
12. R.W. Hasse, Ann. Phys. (NY) 68 (1971) 377-461
13. W.D. Myers, Nukleonika 21 (1976) 3-28
14. K.T.R. Davies and J.R. Nix, Phys. Rev. C14 (1976) 1977-94
15. R.H. Helm, Phys. Rev. 104 (1956) 1466-75
16. G. Süssmann, Z. Phys. A274 (1975) 145-159
17. W.D. Myers, Nucl. Phys. A204 (1973) 465
18. H.J. Krappe, Proc. XIV Masurian Summer School, Mikolajki, September 1981
19. I. Angeli and M. Csatlos, ATOMKI Kozlemenyek 20 (1978) 1
20. F. Touchard, et al., Phys. Lett. 108B (1982) 169
21. H.D. Wohlfahrt, et al., Phys. Rev. C23 (1981) 533
22. A. Andl, et al., Phys. Rev. C26 (1982) 2194
23. H. Gerhardt, et al., Hyperfine Interactions 9 (1981) 175
24. C. Thibault, et al., Phys. Rev. C23 (1981) 2720-9
25. J.W. Lightbody, Jr., et al., Phys. Rev. C14 (1976) 952
26. R. Wenz, A. Timmermann, and E. Matthias, Z. Phys. A303 (1981) 87
27. F. Buchinger, et al., Hyperfine Interactions 9 (1981) 165
28. C. Thibault, et al., Nucl. Phys. A367 (1981) 1-12
29. E.B. Shera, et al., Phys. Lett. 112B (1982) 124
30. A.C. Mueller, et al., Report CERN-EP/82-162

31. R. Neugart, Invited paper to the Conference on Lasers in Nuclear Physics, 21-23 April 1982, Oak Ridge, Tennessee, USA, and Report CERN-EP/82-80, June 1982

32. Ph. Dabkiewicz, Thesis, University Mainz, 1980, unpublished

33. R.C. Thompson, et al., Preprint KfK 3455, Kernforschungszentrum Karlsruhe, FRG, 1982

34. X. Campi and M. Epherre, Phys. Rev. C22 (1980) 2605-8

35. M. Epherre, G. Audi, and X. Campi, Proc. 4th Int. Conf. on Nuclei far from Stability, Helsingor, Denmark, June 1981, p. 62-4

36. F.K. McGowan, et al., Phys. Rev. Lett. 27 (1971) 1741-4

37. R.W. Hasse, Pramāna 11 (1978) 441-55

Appendix

The coefficients C_i in the Legendre polynomial expansion of the Coulomb potential are given by the expressions[37])

$$C_0 = \int_{-1}^{1} d\mu \; S(\mu)^2/2 \quad , \tag{A1}$$

$$C_2 = \int_{-1}^{1} d\mu \; P_2(\mu) \; \ln S(\mu) \quad , \tag{A2}$$

$$C_4 = \int_{-1}^{1} d\mu \; P_4(\mu) \; S(\mu)^{-2}/(-2) \quad , \tag{A3}$$

$$C_6 = \int_{-1}^{1} d\mu \; P_6(\mu) \; S(\mu)^{-4}/(-4) \quad , \tag{A4}$$

etc.

where

$$S(\mu) = 1 + \alpha_2 P_2(\mu) + \alpha_4 P_4(\mu) + \alpha_6 P_6(\mu) + \ldots \quad . \tag{A5}$$

If (as elsewhere) we retain terms up to order ϵ^4 and regard α_2, α_4, and α_6 as being of relative order ϵ, ϵ^2, and ϵ^3, these coefficients are

$$C_0 = 1 + \frac{1}{5}\alpha_2^2 + \frac{1}{9}\alpha_4^2 + \ldots \tag{A6}$$

$$C_2 = \frac{2}{5}\alpha_2 - \frac{2}{35}\alpha_2^2 + \frac{2}{35}\alpha_2^3 - \frac{2}{77}\alpha_2^4 - \frac{4}{35}\alpha_2\alpha_4 + \frac{24}{385}\alpha_2^2\alpha_4 - \frac{20}{693}\alpha_4^2 + \ldots \tag{A7}$$

$$C_4 = -\frac{6}{35}\alpha_2^2 + \frac{48}{385}\alpha_2^3 - \frac{204}{1001}\alpha_2^4 + \frac{2}{9}\alpha_4 - \frac{40}{231}\alpha_2\alpha_4 + \frac{7156}{15015}\alpha_2^2\alpha_4 - \frac{54}{1001}\alpha_4^2 - \frac{30}{143}\alpha_2\alpha_6 + \ldots \tag{A8}$$

$$C_6 = \frac{180}{1001}\alpha_2^3 - \frac{36}{143}\alpha_2^4 - \frac{50}{143}\alpha_2\alpha_4 + \frac{540}{1001}\alpha_2^2\alpha_4 - \frac{100}{1287}\alpha_4^2 + \frac{2}{13}\alpha_6 + \ldots \tag{A9}$$

The coefficients D_i in the expansion of $\tilde{v}$ (eq. (15)) are equal to the corresponding coefficients C_i except for D_0, which is

$$D_0 = \frac{1}{5} + \frac{1}{25}\alpha_2^2 - \frac{432}{6125}\alpha_2^4 + \frac{8}{175}\alpha_2^2\alpha_4 + \frac{11}{135}\alpha_4^2 + \cdots \quad . \tag{A10}$$

Figure Captions

Fig. 1. The difference between the measured RMS charge radius and the Droplet Model predictions of eq. (21). The points are plotted against neutron number, and members of the same isotopic sequence are connected by a line.

Fig. 2. The same as fig. 1 but without corrections for deformation.

Fig. 3. The same as fig. 1 but using the Liquid Drop Model expression of eq. (25) with deformation corrections instead of the Droplet Model.

Fig. 4. The slope ΔR_n of the equivalent sharp charge radius versus neutron number multiplied by $A^{2/3}$ is plotted against the charge number of the isotopic sequence being considered. The dashed line is the Droplet Model prediction, and the dotted line is the Liquid Drop Model prediction.

Fig. 5. The measured mean square charge radii (relative to N = 80) of the cesium isotopes are plotted as solid circles and connected by a line. The solid triangles correspond to the full Droplet Model prediction with calculated deformation corrections included. The dashed line corresponds to the uncorrected Droplet Model and the dot-dashed line corresponds to the uncorrected Liquid Drop Model.

Fig. 6. The measured mean square charge radii (relative to N = 50) of the rubidium isotopes are plotted as solid circles and connected by a line. The solid triangles correspond to the full Droplet Model prediction with calculated deformation corrections included. The dashed line corresponds to the uncorrected Droplet Model and the dot-dashed line corresponds to the uncorrected Liquid Drop Model.

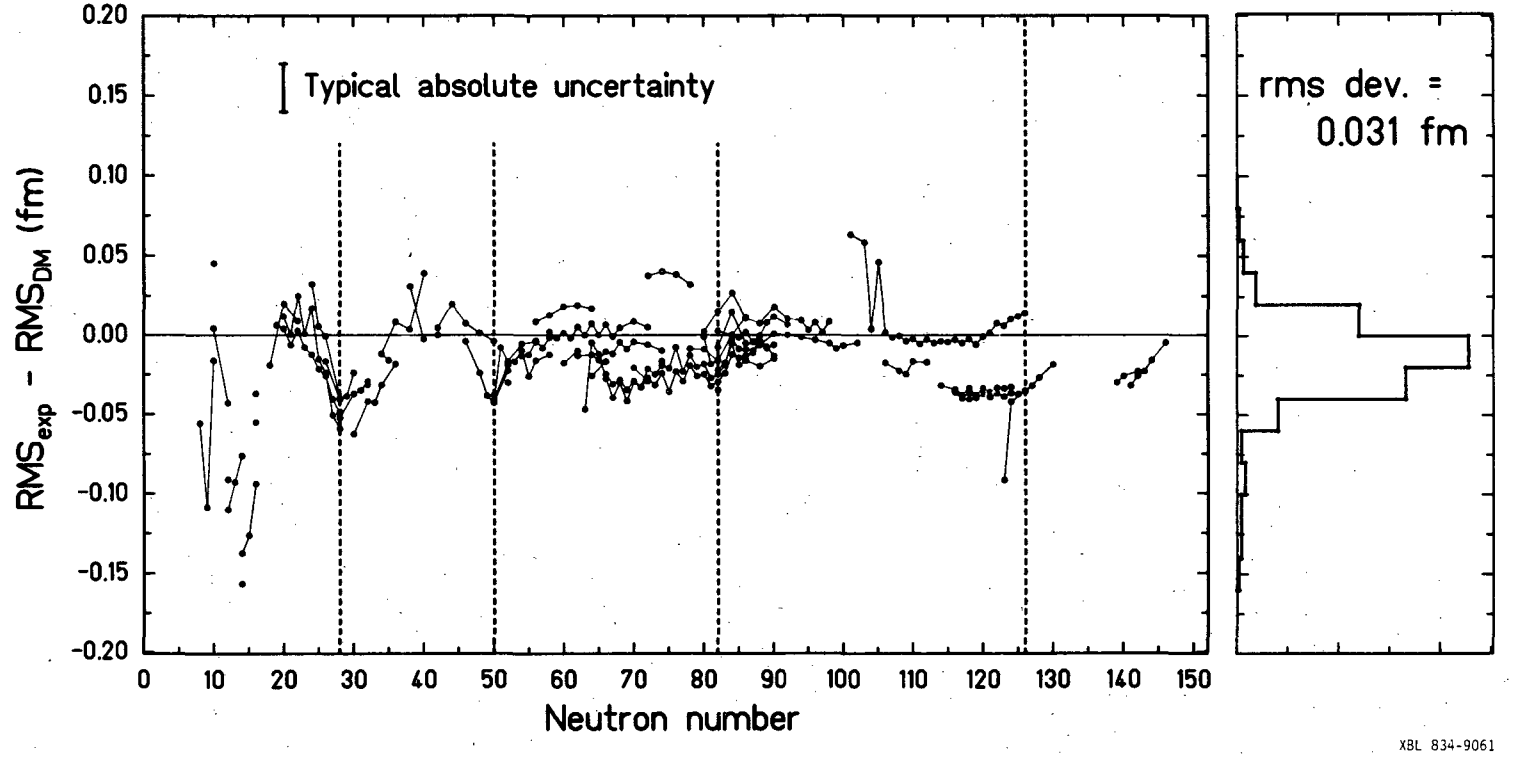
Typical absolute uncertainty
rms dev. =
0.031 fm
RMS$_{exp}$ - RMS$_{DM}$ (fm)
Neutron number
0.20
0.15
0.10
0.05
0.00
-0.05
-0.10
-0.15
-0.20
0
10
20
30
40
50
60
70
80
90
100
110
120
130
140
150
XBL 834-9061

Fig. 1.

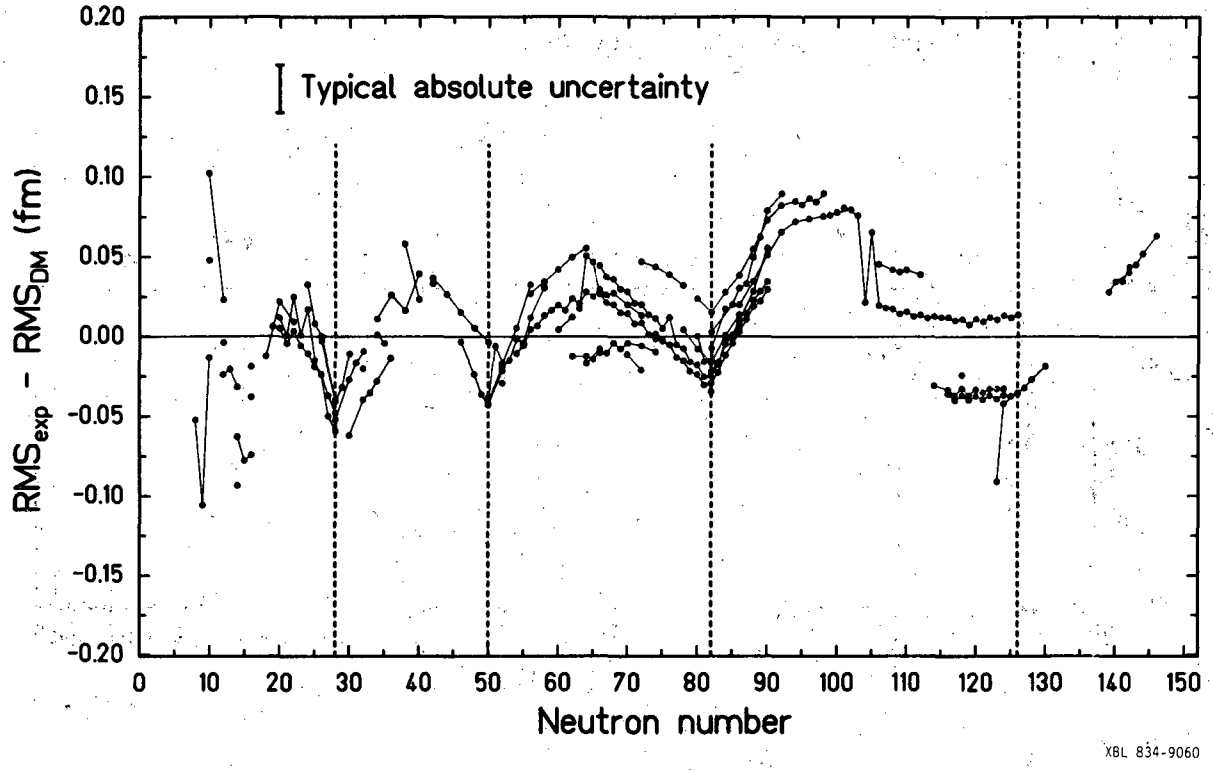
Typical absolute uncertainty
RMS$_{exp}$ - RMS$_{DM}$ (fm)
Neutron number
0.20
0.15
0.10
0.05
0.00
-0.05
-0.10
-0.15
-0.20
0
10
20
30
40
50
60
70
80
90
100
110
120
130
140
150
XBL 834-9060

Fig. 2.

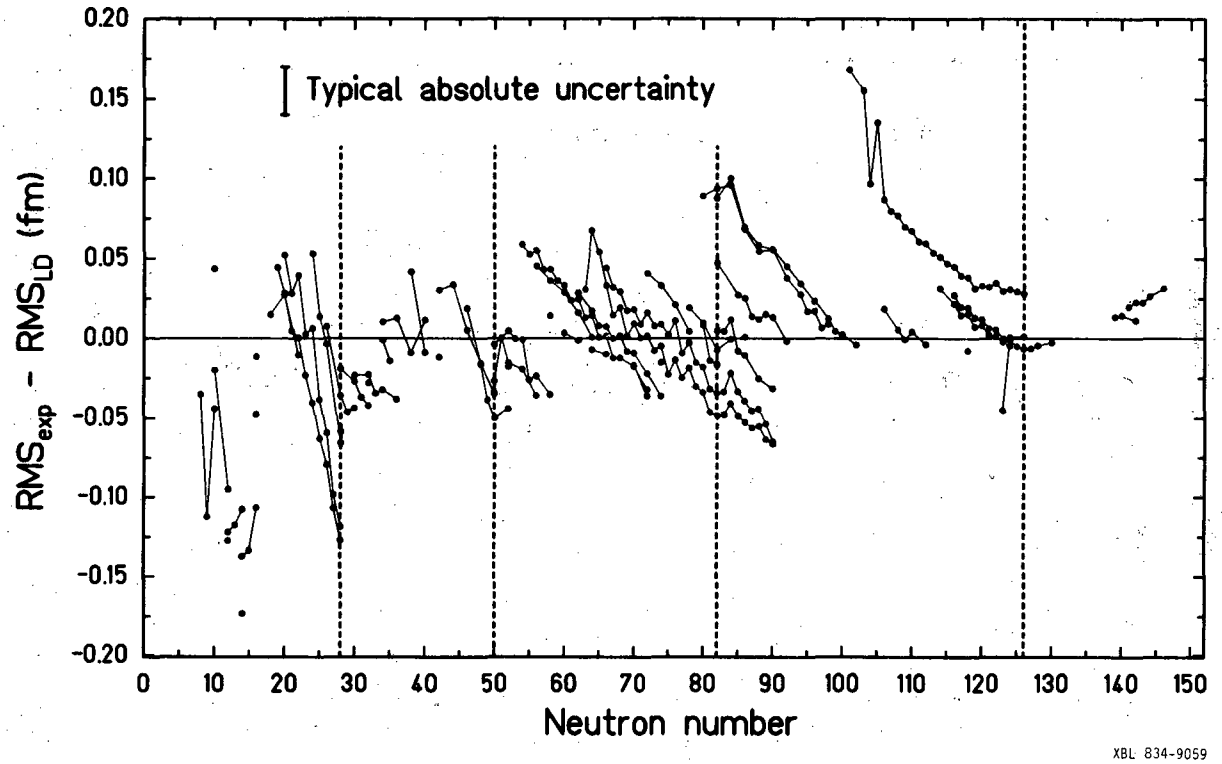
Typical absolute uncertainty
$RMS_{exp} - RMS_{LD}$ (fm)
Neutron number
0.20
0.15
0.10
0.05
0.00
-0.05
-0.10
-0.15
-0.20
0
10
20
30
40
50
60
70
80
90
100
110
120
130
140
150
XBL 834-9059

Fig. 3.

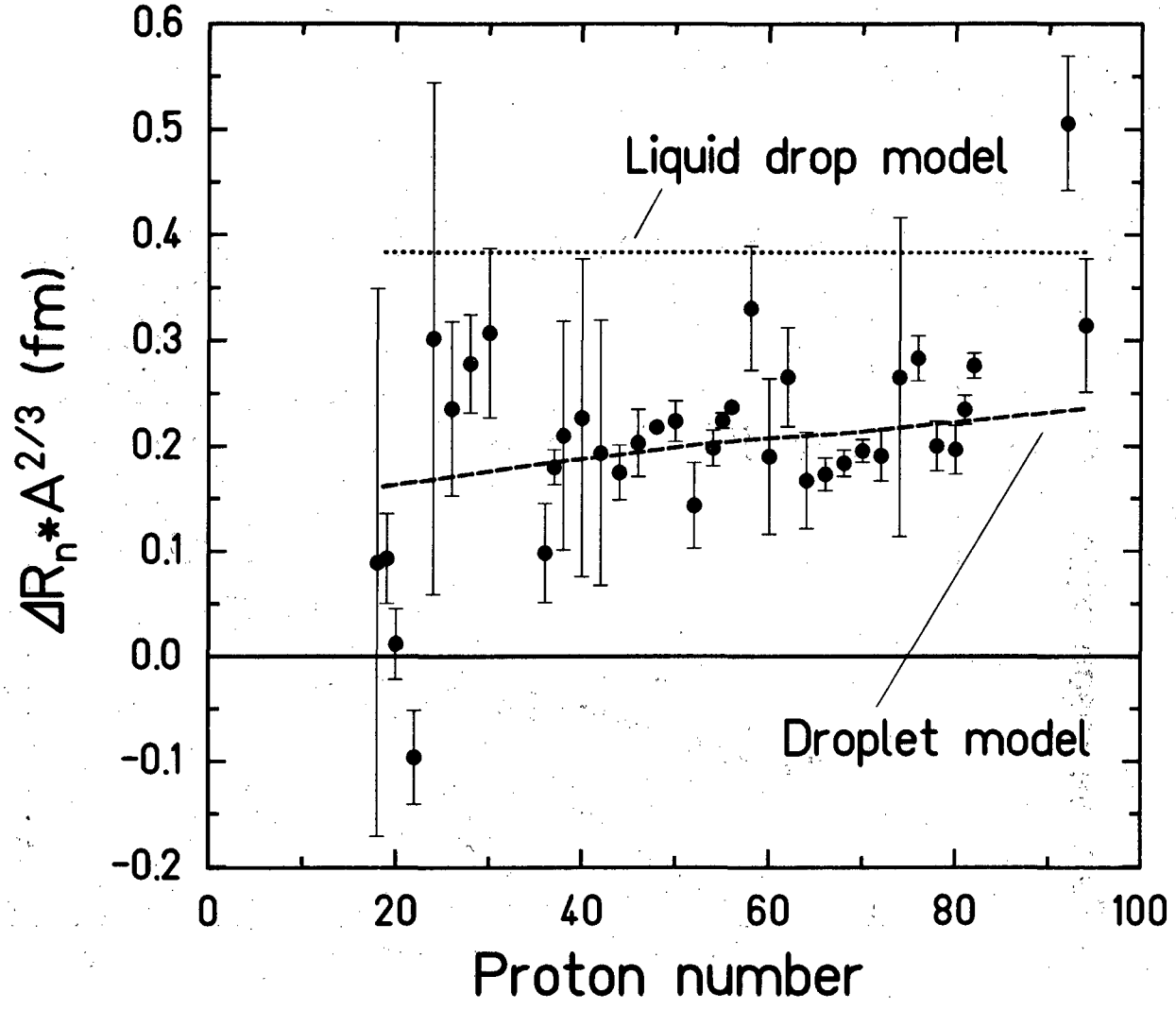

XBL 834-9062

Fig. 4.

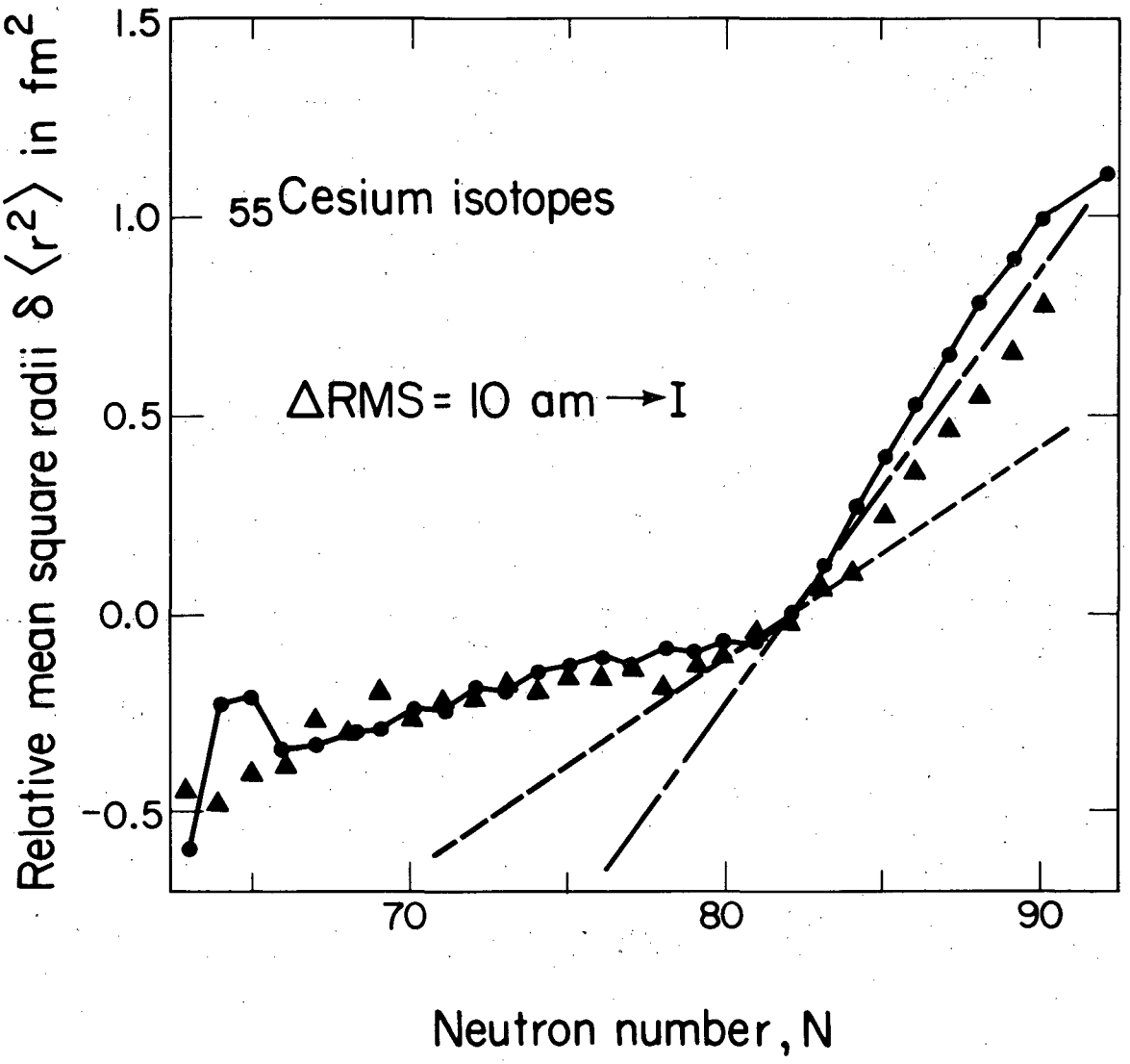

XBL 834-9063

Fig. 5.

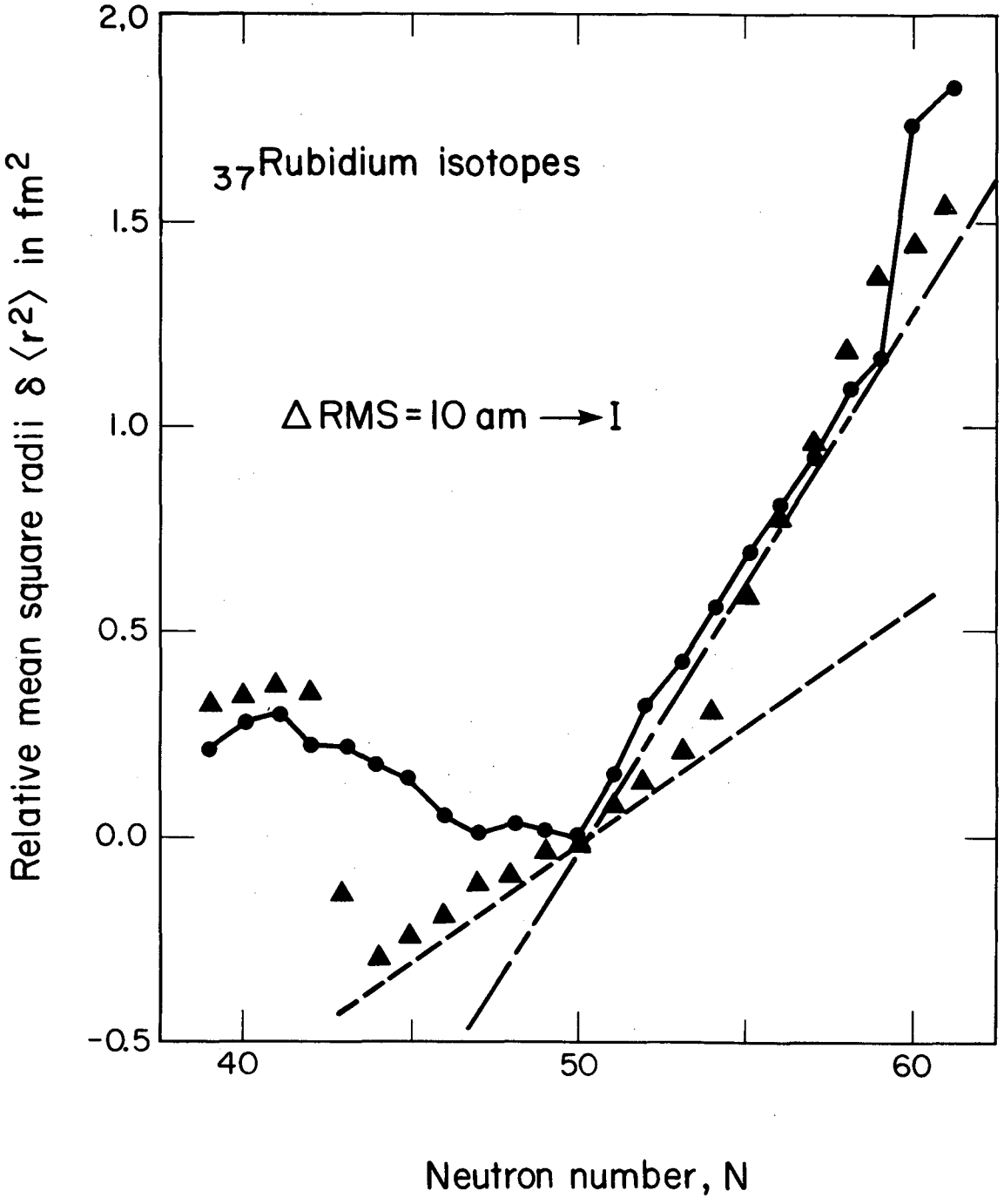

XBL 834-9064

Fig. 6.

TECHNICAL INFORMATION DEPARTMENT
LAWRENCE BERKELEY LABORATORY
UNIVERSITY OF CALIFORNIA
BERKELEY, CALIFORNIA 94720